Electronic Supplementary Information (ESI) for Nanoscale

$Ti_3C_2T_x$ MXene augments osmo-adaptive repression of the inflammatory stress response for improved wound repair

Sertan Kiziloz [1*], Emma J. Ward [1*], Daniel Hawthorne [1], Avick Sinha [1,2], Grace Cooksley [3], Dipak Sarker [1], Cyril Crua [4], Andrew Lloyd [1], Christopher E. Shuck [5], Yury Gogotsi [6], Susan Sandeman [1**]

[1] Centre for Regenerative Medicine and Devices, School of Applied Sciences, University of Brighton, Brighton BN2 4GJ, UK.

[2] Advanced Engineering Centre, University of Brighton, Brighton BN2 4GJ, UK.

[3] Developmental Biology and Cancer (DBC) Research and Teaching Department, UCL GOS Institute of Child Health, London WC1N 1EH, UK.

[4] School of Engineering and Informatics, University of Sussex, Brighton, BN1 9QJ, UK.

[5] Department of Chemistry and Chemical Biology, Rutgers University, Piscataway, NJ 08854, USA.

[6] Department of Materials Science and Engineering and A. J. Drexel Nanomaterials Institute, Drexel University, Philadelphia, PA 19104, USA.

*Joint first authors

**Corresponding author s.sandeman@brighton.ac.uk

```
clc;clear ;close all

% Detetction of edge
%----------------------------------------
Step 1 load image of drop
%----------------------------------------

dname="C:\Users\as3792\Downloads\OneDrive_2024-07-01 Mannitol Glycine Betaine MXene_Scratch_HaCaT_Mannitol_GB_Velocity\';
count=1;

ima=193 % Image number
im=(imread([dname 'Image_' num2str(ima-1) '.JPEG'])); %loads image
%Sharpen and increase contrast of image
figure; imshow(im); b0=im2gray(im);
b1-medfilt2(im2double (b0), [5 5]); figure; imshow(b1);
b3-adapthisteq(b1); figure; imshow(b3);
b4 = edge(b3, 'canny',.35); figure; imshow(b4);
b4a(1:960,:)=medfilt2(b4(:,:),[2 2]); %from 2 hrs

sel strel('disk',15); %T0- 10
C0-imclose(b4a, sel); figure; imshow(C0);

C1-imfill(C0,1, 'holes'); figure; imshow(C1);
C3-bwareaopen(C0,4500); figure; imshow(C3);

C3a=C3(:,1:480); C3b=C3(:,480:960);
C7t0-edge (C3a(:, :),"canny"); figure; imshow(C7t0);
[LX1 LY1] find(C7t0);
c8t0-edge (C3b(:,:), "canny"); figure; imshow(C8t0);
[LX2 LY2]= find(C8t0);

[rowl,coll] find (C7t0); [rown, colr] find (C8t0);
d1= accumarray(rowl, coll, [size(C7t0,1),1], @max, NaN); % left side
d2= accumarray(rowr, colr, [size(C8te,1),11,@min, NaN); % right side
```

ESI Figure 1 Custom MATLAB code developed in house for the wound healing model

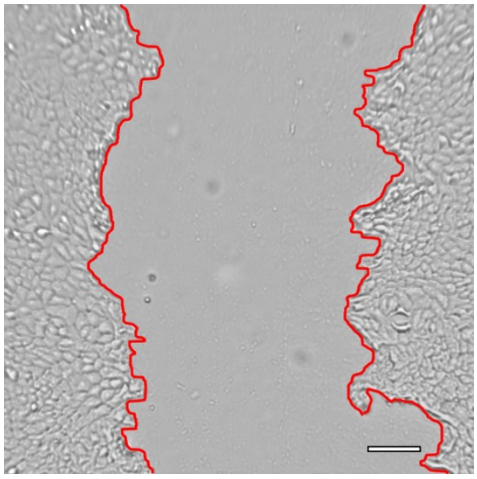

ESI Fig 2 – Example scratch assay micrograph showing HaCaT keratocytes migrating towards the scratched area with the red outlines marking the HaCaT cell edges. Edge detection algorithms in MATLAB were used to generate contours and precisely trace the boundary between the migrating cells and the cell-free zone. Scale bar = 100 µm.

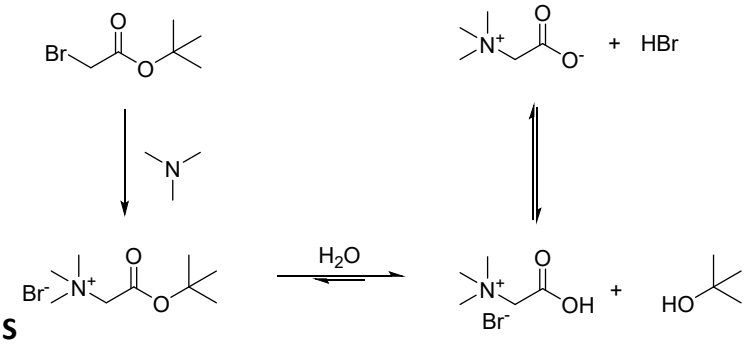

S

ESI Fig 3 – A reaction scheme for the synthesis of 2-(tert-butoxy)-N,N,N-trimethyl-2-oxoethan-1-aminium (tBu-GB) bromide, and its hydrolytic degradation to release free GB.

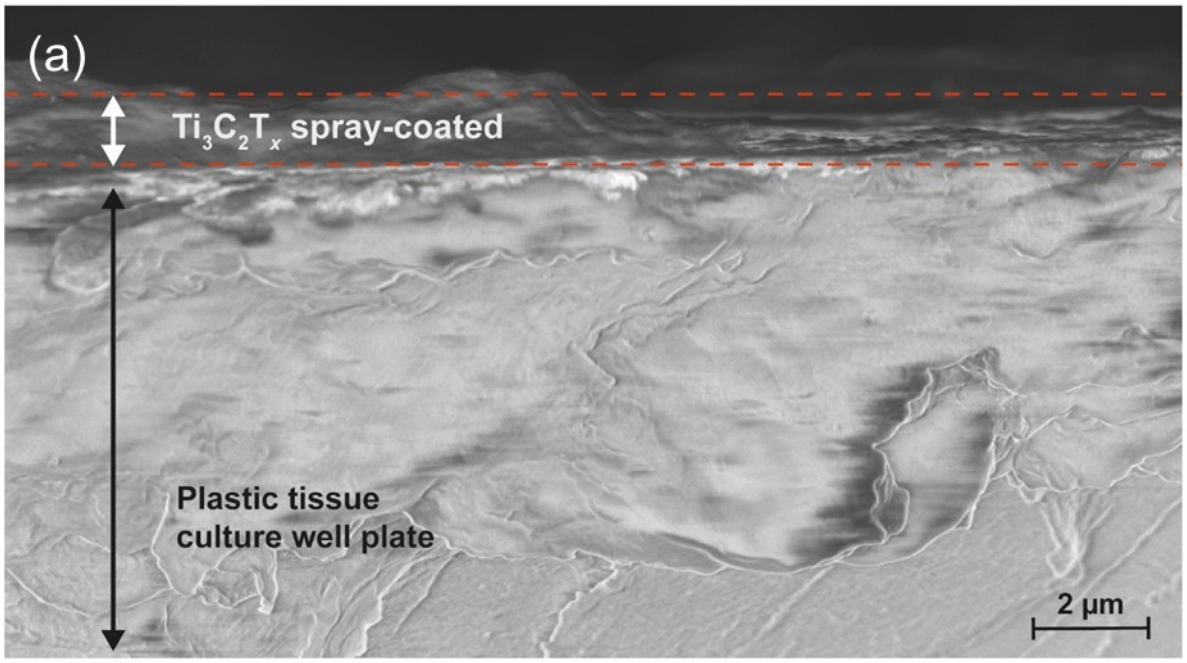

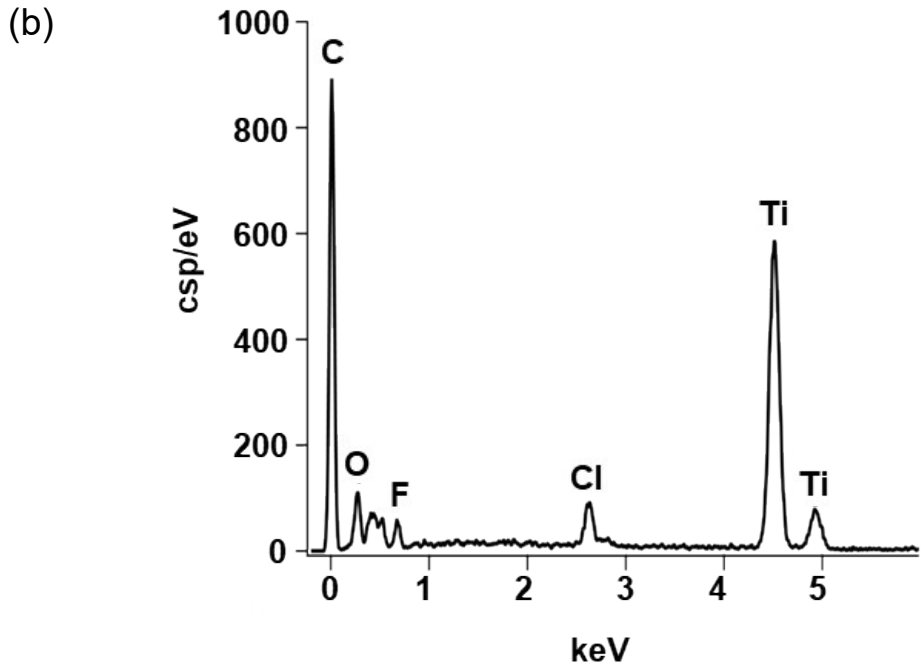

ESI Fig 4 – (a) Scanning electron microscopy (SEM) image of $Ti_3C_2T_x$ spray-coated onto tissue culture plates. Samples were prepared and mounted to the side of a hexagonal nut perpendicular to the electron beam. High-resolution images were produced using a field emission SEM (Zeiss Sigma, Germany) with a 1.5 kV accelerating voltage. (b) Energy dispersive x-ray spectroscopy (EDX) spectrum confirming the presence and elemental composition of the $Ti_3C_2T_x$ coating.

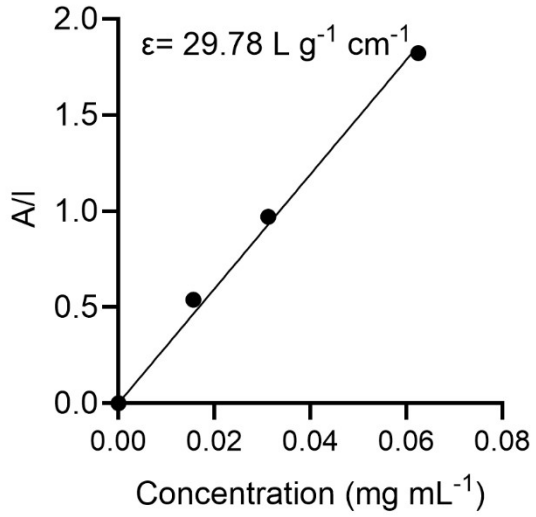

ESI Fig 5 – UV-Vis calibration curve of $Ti_3C_2T_x$ colloidal solutions, where the molar extinction coefficient was calculated as 29.78 L g-1 cm-1 following Beer-Lambert's Law.

ESI Table 1 – Root Mean Square Error (RMSE) and R^2 values for wound closure model across different conditions (cell only, mannitol, mannitol GB) with and without $Ti_3C_2T_x$ coating.

	Cell only		**Mannitol**		**Mannitol GB**	
	Uncoated	$Ti_3C_2T_x$	Uncoated	$Ti_3C_2T_x$	Uncoated	$Ti_3C_2T_x$
RMSE	0.041	0.024	0.011	0.024	0.016	0.016
R^2	0.995	0.998	0.996	0.998	0.999	0.998

ESI Table 2 – Rate coefficients of wound closure data. The rate coefficient *b***,** along with its standard error, derived from the curve fit with a 95% confidence level, was determined for the cell-only, mannitol, and mannitol-GB treated conditions.

Coefficient *b*

	Uncoated	**$Ti_3C_2T_x$**
Cell only	0.139 ±0.07	0.179±0.09
Mannitol	0.047±0.02	0.075±0.03
Mannitol GB	0.019±0.01	0.124±0.06

ESI Table 3 – Rate coefficient of wound closure data. The rate coefficient *c* along with its standard error, derived from the curve fit with a 95% confidence level, was determined for the cell-only, mannitol, and mannitol-GB treated conditions.

Coefficient *c*

	Uncoated	**$Ti_3C_2T_x$**
Cell only	0.668±0.34	0.851±0.43
Mannitol	1.796±0.91	0.866±0.44
Mannitol GB	2.380±1.21	0.760±0.38

ESI Table 4 – The Migratory velocity values for the wound closure model, as mean µm/s ± SD.

Time / hour	Cell Only	$Ti_3C_2T_x$	Mannitol	$Ti_3C_2T_x$ Mannitol	Mannitol GB	$Ti_3C_2T_x$ Mannitol GB
0	0	0	0	0	0	0
2	0.0181 ±0.0032	0.0221 ±0.0017	0.014 ±0.0021	0.0177 ±0.0015	0.0172 ±0.0019	0.0206 ±0.0015
4	0.0175 ±0.0025	0.0187 ±0.0018	0.01 ±0.0019	0.0181 ±0.001	0.0123 ±0.0014	0.0138 ±0.001
8	0.0164 ±0.002	0.0116 ±0.0005	0.0063 ±0.002	0.0075 ±0.0005	0.0082 ±0.001	0.0085 ±0.0005
12	0.014 ±0.0015	0.0031 ±0.0005	0.0066 ±0.002	0.0041 ±0.001	0.0069 ±0.0015	0.0056 ±0.0015
24			0.0033 ±0.0007	0.0035 ±0.0002	0.0043 ±0.0006	0.0031 ±0.0002
36			0.0024 ±0.0002		0.0035 ±0.0006	
48			0.0011 ±0.0003		0.0019 ±0.0009	

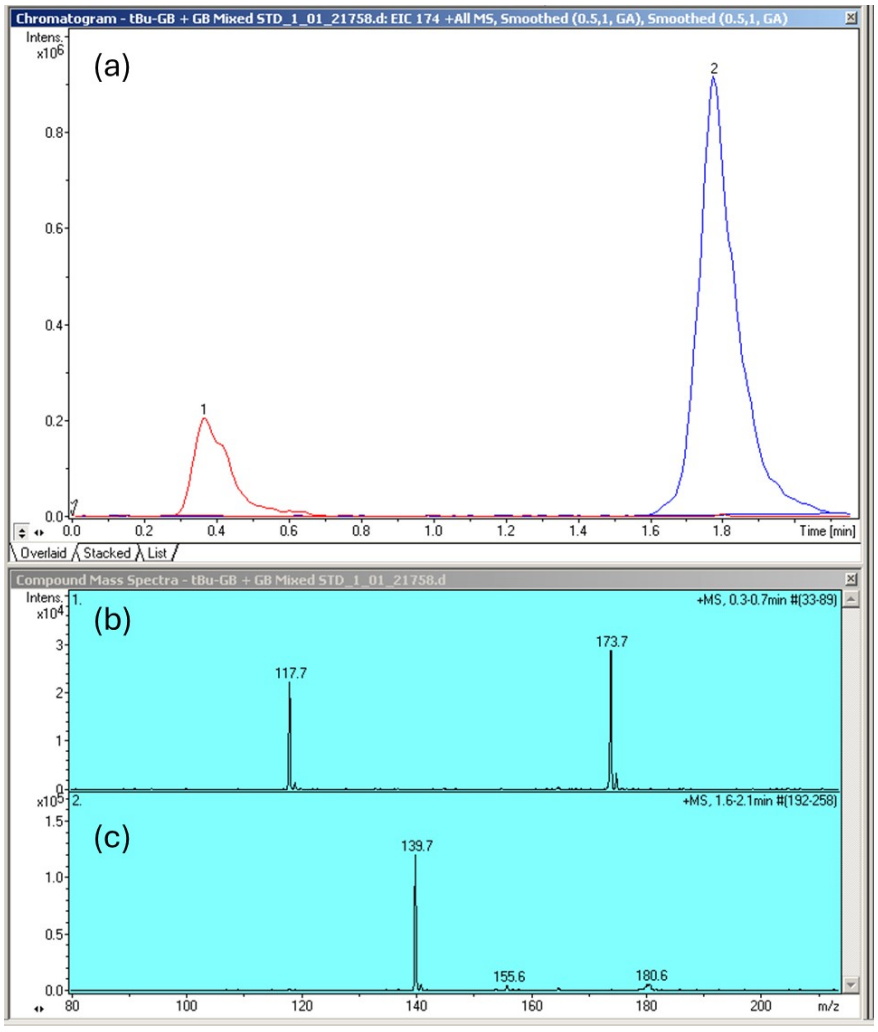

ESI Fig 6 – Example chromatogram and mass spectra produced by High-Performance Liquid Chromatography tandem Mass Spectrometry (HPLC-MS) analysis to detect GB and tBu-GB by molecular mass. These images are provided as examples only to illustrate the retention times and *m/z* values of the compounds of interest. Peak integral data from chromatography was extracted and used to construct time vs. elution plots. (a) A representative chromatogram of

a mixed GB/tBu-GB standard injected into the HPLC-MS system showing an indicative retention time of 0.35 min for tBu-GB and 1.9 min for GB. (b) Mass spectrum corresponding to tBu-GB. (c) Mass spectrum corresponding to GB. The chromatographic for tBu-GB identified 2 peaks corresponding to tBu-GB with a mass spectrum dominated by the molecular ion peak, 174 m/z; and another, smaller peak at 118 m/z. The latter corresponds to a proton adduct of GB, $[H•GB]^{+\cdot}$. Presumably, ester scission to generate GB has occurred in the MS ionisation source, since a commercial authentic GB sample elutes at 1.9 min and with a mass spectrum dominated by a peak at 140 m/z, which corresponds to its sodium adduct.

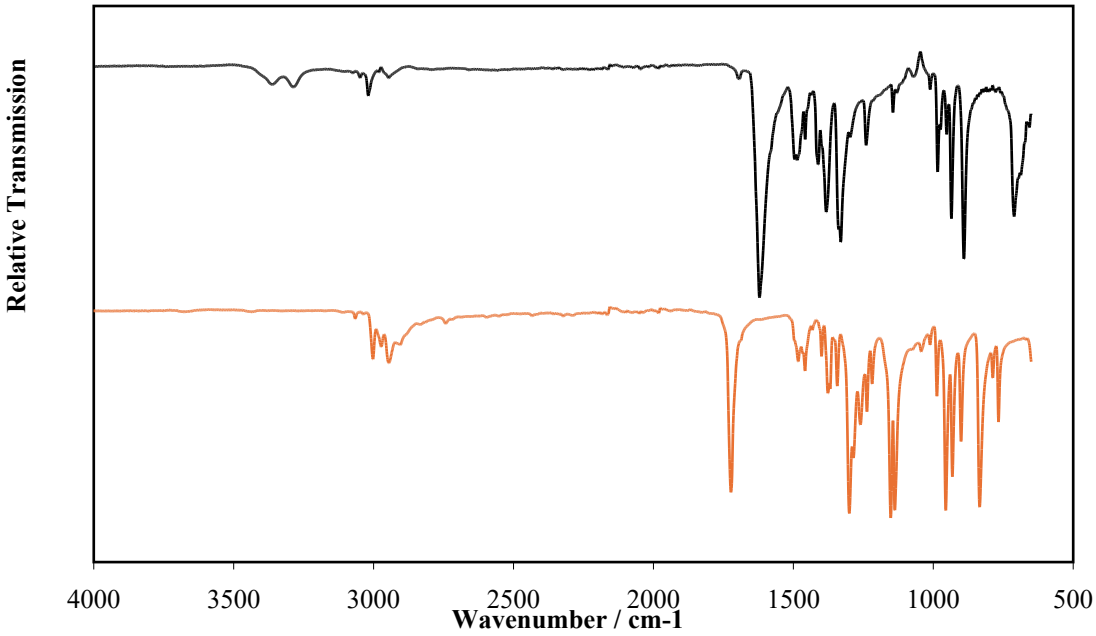

ESI Fig 7 – FTIR spectra of GB and tBu-GB, recorded from a commercial sample of GB (black trace) and synthesised tBu-GB (orange trace). The betaine inner salt carboxylate peak appears at 1622 cm^{-1}, in agreement with the literature.[1] For tBu-GB, this peak is at 1722 cm^{-1}, which is similar to the FTIR spectra of other betaine esters found in the literature. [2] The presence of the tert-butyl ester is also revealed by the sharp peak at 1151 cm^{-1} (C-O-C) and the series of C-H alkyl peaks at 2800 – 3000 cm^{-1}. These peaks are absent in the GB spectrum.

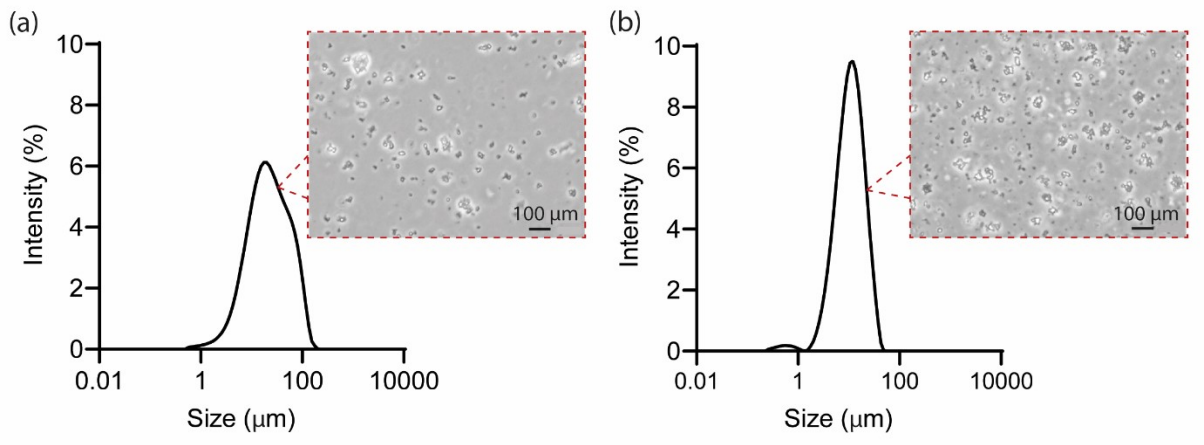

ESI Fig 8 – Polyacrylate microgel sizing data before and after loading with tBu-GB. Particle size analysis was carried out using dynamic light scattering (Mastersizer 3000, Malvern, UK) and indicated limited changes in size and dispersity on microgel loading with tBu-GB (a) DLS sizing data for non-tBu-GB loaded plain polyacrylate microgels with an insert micrograph image showing the non-tBu-GB loaded gels at X40 magnification ; (b) DLS sizing data for tBu-GB loaded gels with an insert micrograph image of the tBu-GB loaded gels at x40 magnification.

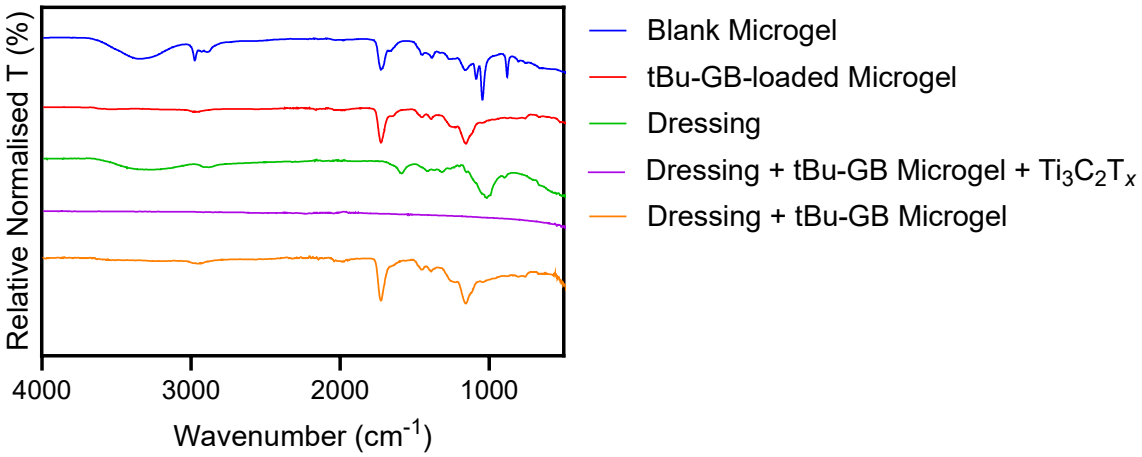

ESI Fig 9 – FTIR analysis of the polyacrylate microgels pre- and post-loading with tBu-GB compared to the blank and $Ti_3C_2T_x$-tBu-GB-microgel dressing. Normalised and offset FTIR analysis spectra of the polyacrylate microgels and microgel/ $Ti_3C_2T_x$-coated dressing showing blank microgels (blue trace), tBu-loaded microgels (red trace), unmodified dressing (green trace), $Ti_3C_2T_x$-coated dressing, outer surface (purple trace), tBu-GB Microgel loaded dressing, inner layer (orange trace). FTIR spectra have been normalised and offset according to the following equation (1)

$$\%T_f = 100 - (a \times (100 - \%T_i) + c \quad (1)$$

where $\%T_f$ is the plotted transmission, $\%T_i$ is the raw transmission value, and *a* is an arbitrary normalising constant selected to best enhance visibility of peaks in samples whose overall $\%T_i$ was low, and *c* is an arbitrary offset value selected to prevent spectral overlap on the y axis.

FTIR spectral analysis of the microgels with and without tBu-GB loading shows that the electrostatic loading of (cationic) tBu-GB into (anionic) AA-based gels was successful. Due to the overlap of the peaks relating to the carbonyl groups in AA, EGDMA, and tBu-GB, it is difficult to assign the success of the tBu-GB incorporation based on the carbonyl peak(s) alone. Nonetheless, the spectrum of the non-loaded AA/EGDMA gels is characterised by a broad peak at 3300–3500 cm^{-1}, which correlates to a -OH stretching vibration in a strongly hydrogen bonded environment; this is likely due to interactions of COOH groups in the dry gel with one another. This broad band disappears almost entirely once the tBu-GB has been incorporated into the gels, thus implying that the strongly H-bonded environment no longer persists. This is readily explained by the deprotonation of the AA COOH groups during the ion exchange loading process (during which H^+ and Cl^- are removed from the gel and tBu-GB, respectively, as HCl (aq.), by water washing). The deprotonated carboxylate group is no longer able to act as a hydrogen bond donor, thus the peak disappears. A simplified chemical equation for the ion exchange loading process is shown below in equation 2.

$$\cdots COO^- H^+ + \cdots N^+ Me_3\, Cl^- \leftrightharpoons \cdots COO^- N^+ Me_3 \cdots + HCl \qquad (2)$$

FTIR spectral analysis of the cellulosed based commercial dressings in $Ti_3C_2T_x$-coated and GB-eluting microgel embedded forms indicate a successful modification of the dressing. In the $Ti_3C_2T_x$-coated sample, the classical cellulosic FTIR spectrum of the dressing, with its cluster of peaks around 1100 (related to C-O ether/alcohol functionality), is almost entirely masked by $Ti_3C_2T_x$. The masking of any of the original dressing peaks indicates that the inorganic coating has completely coated the dressing's outer surface. The inner layer of dressing which was loaded with tBu-GB-loaded microgel displays features of both the modified dressing and the microgels, with a strong carbonyl stretching vibration correlating to the gels, while the cellulose alcohol and ether-related peaks remain (albeit somewhat reduced in intensity) in the 1000–1200 cm^{-1} region. This indicates a successful incorporation of the gels primarily onto the surface of, but also potentially penetrating within, the fibrous dressing structure.

References

1. T. I. Youji Kitamura, Madoka Saito, Masaki Mifune, Yutaka Saito, Kyoko Sato, Chikako Yomota, Kenichi Tanamoto, *jstage*, 2006, **47**, 232-236.

2. N. A. Efiana, G. Kali, A. Fürst, A. Dizdarević and A. Bernkop-Schnürch, *European Journal of Pharmaceutical Sciences*, 2023, **180**, 106313.